JOURNAL OF GEOPHYSICAL RESEARCH, VOL. 98, NO. A12, PAGES 21,163–21,176, DECEMBER 1, 1993

Bernstein Waves in the Io Plasma Torus: A Novel Kind of Electron Temperature Sensor

NICOLE MEYER-VERNET, SANG HOANG, AND MICHEL MONCUQUET

Département de Recherche Spatiale, Centre National de la Recherche Scientifique, Observatoire de Paris, France

During Ulysses passage through the Io plasma torus, along a basically north-to-south trajectory crossing the magnetic equator at $R \sim 7.8\ R_J$ from Jupiter, the Unified Radio and Plasma Wave experiment observed weakly banded emissions with well-defined minima at gyroharmonics. These noise bands are interpreted as stable electrostatic fluctuations in Bernstein modes. The finite size of the antenna is shown to produce an apparent polarization depending on the wavelength, so that measuring the spin modulation as a function of frequency yields the gyroradius and thus the local cold electron temperature. This determination is not affected by a very small concentration of suprathermal electrons, is independent of any gain calibration, and does not require an independent magnetic field measurement. We find that the temperature increases with latitude, from $\sim 1.3 \times 10^5$ K near the magnetic (or centrifugal) equator, to approximately twice this value at $\pm 10°$ latitude (i.e., a distance of $\sim 1.3\ R_J$ from the magnetic equatorial plane). As a by-product, we also deduce the magnetic field strength with a few percent error.

1. INTRODUCTION

During the Jovian flyby of Ulysses the spacecraft traversed the outer part of Io's "warm" plasma torus. The Unified Radio and Plasma Wave (URAP) experiment [*Stone et al.*, 1992*a*] observed, among a complex spectrum of waves, continuous emissions near the upper hybrid frequency and between consecutive harmonics of the electron gyrofrequency. In the densest traversed region the electron density was high enough for the upper hybrid frequency to be close to the plasma frequency, and the noise spectrum background in that frequency range often corresponds to that of quasi-thermal fluctuations [*Meyer-Vernet and Perche*, 1989], from which the plasma density and, less straightforwardly, the temperature of the cold electrons can be derived [*Stone et al.*, 1992*b*; S. Hoang et al., Electron density and temperature in the Io plasma torus from Ulysses thermal noise measurements, submitted to *Planetary and Space Science*, 1993 (hereinafter referred to as Hoang et al., submitted manuscript, 1993)].

We focus in this paper on the emissions peaking in intensity between consecutive gyroharmonics. They are generally weak, except in the close vicinity of Jupiter's magnetic equatorial plane. Similar weakly banded emissions have been observed in the magnetospheres of Earth [e.g., *Shaw and Gurnett*, 1975; *Christiansen et al.*, 1978], Jupiter [*Kurth et al.*, 1980], Saturn [*Kurth et al.*, 1983], Uranus [*Kurth et al.*, 1987], and in the Io plasma torus [*Birmingham et al.*, 1981]. They are generally called "$(n + 1/2)f_g$" emissions, even though their maximum amplitude is not necessarily observed at the center of a band. Although they have often been attributed to plasma instabilities, *Sentman* [1982] has shown that at least those observed in the dayside magnetosphere of the Earth can be interpreted as quasi-thermal fluctuations in Bernstein waves.

We shall calculate the apparent polarization (i.e., the variation of the spectral density with the antenna orientation), a problem not addressed by Sentman, for Bernstein waves "seen" by Ulysses long dipole antenna. We will show that it has a rather unexpected behavior which agrees with the observations; from its analysis, the electrostatic wavelength and thus the cold electron temperature can be derived. We shall also compare the maximum level with a theoretical estimate of quasi-thermal noise using the work of *Sentman* [1982].

Paper number 93JA02587.
0148-0227/93/93JA-02587$05.00

2. OBSERVATIONS

The observations were carried out with the URAP radio astronomy receivers [*Stone et al.*, 1992*a*], connected to the 2×35 m electric field dipole antenna located in the spacecraft spin plane. The spacecraft is spin-stabilized with a spin period of 12 s. During the torus crossing the low-frequency receiver was linearly swept through 64 equally spaced frequency channels (of bandwidth 0.75 kHz) covering the range 1.25–48.5 kHz in 128 s. The high-frequency receiver sweeps through 12 frequency channels (of bandwidth 3 kHz) in the range 52–940 kHz.

2.1. *Overview*

Figure 1 is a radio spectrogram acquired during the torus traversal and farther out from Jupiter, displayed as frequency versus time, with relative intensity indicated by increasing darkness. The lower panel shows the data from the low-frequency receiver; the upper panel shows the data from both receivers. The increase in intensity seen from ~1800 UT to ~2115 UT outside the torus corresponds to a change in the antenna-receiver operating mode. The periodic white vertical bars are interruptions of the observations due to the operation of the relaxation sounder. The time interval displayed begins ~2 hours after closest approach, at Jovicentric distance $\sim 6.7\ R_J$ and magnetic latitude ~27° north, and ends at distance $\sim 12.6\ R_J$ and magnetic latitude ~8° south (based on an approximate tilted dipole model). The dark smear near 1616 UT between f_g and $2f_g$ corresponds to enhanced noise associated with magnetic equator crossing (see section 2.3).

We have superimposed the plasma frequency f_p, as deduced from the noise near the upper hybrid frequency f_{UH}

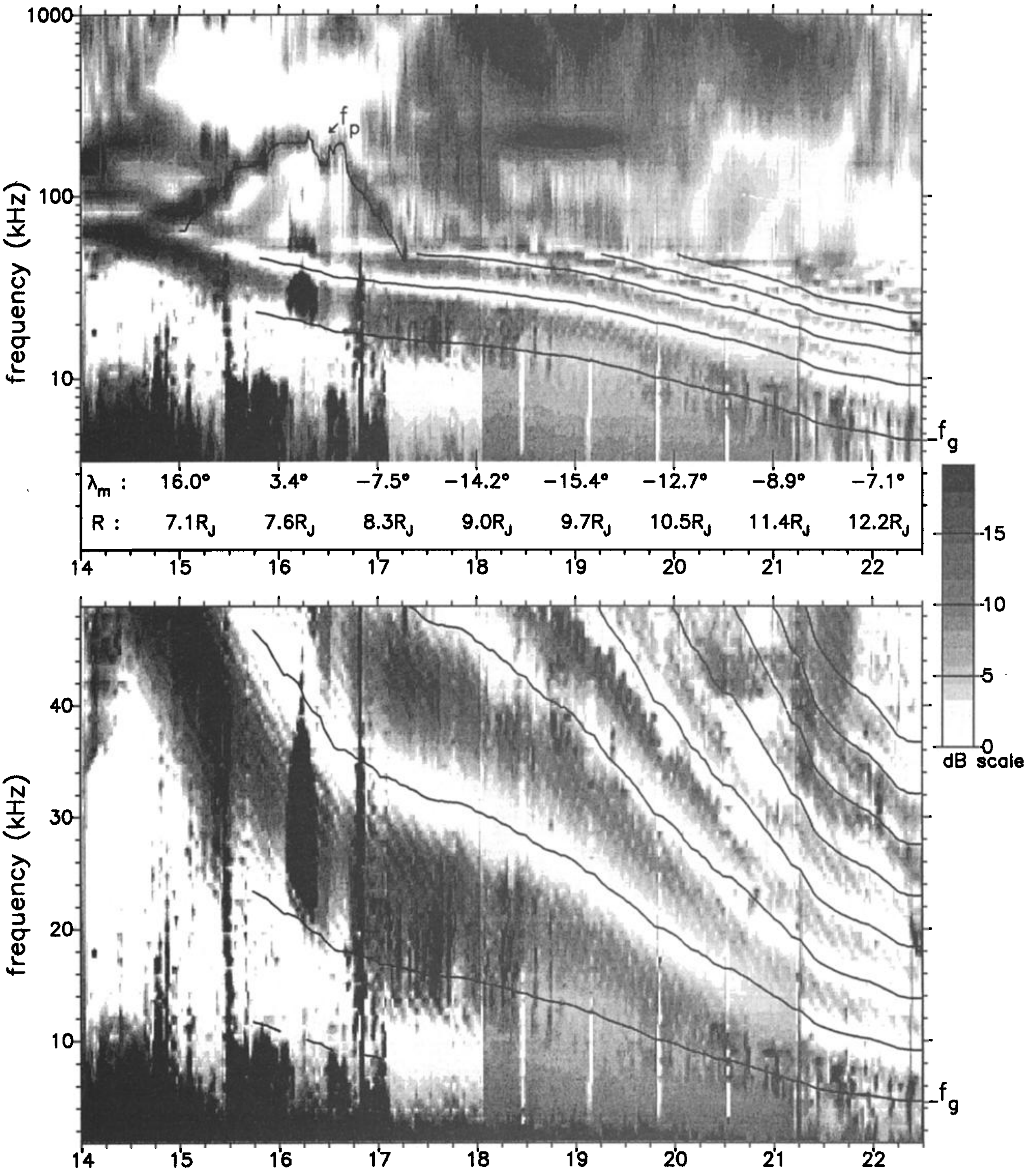

Fig. 1. Unified radio and plasma wave dynamic spectrum during encounter displayed as frequency versus time, with relative intensity indicated by the bar chart on the right. The torus traversal took place near 1400–1800 UT. We have superimposed in continuous lines the plasma frequency f_p deduced from the upper hybrid noise and harmonics of the electron gyrofrequency f_g (calculated from the data as explained in section 4.3). The distance to Jupiter R (in Jovian radii) and magnetic latitude λ_m are given in the middle panel. The dashed line near 1600 UT in the lower panel shows $f_g/2$ (see text).

when $f_{UH} \approx f_p$, and a few harmonics of the electron gyrofrequency f_g calculated as explained in section 4.3 (which deviates by only a few percent from the onboard magnetometer data [*Balogh et al.*, 1992]). These frequencies are related to the plasma density n_e and magnetic field strength B by $f_p \approx 9n_e^{1/2}$, $f_g \approx 2.8 \times 10^{10}\ B$, $f_{UH} = (f_p^2 + f_g^2)^{1/2}$ in S.I. units. Some bursty emissions can be seen near and below the gyrofrequency; in most of the densest

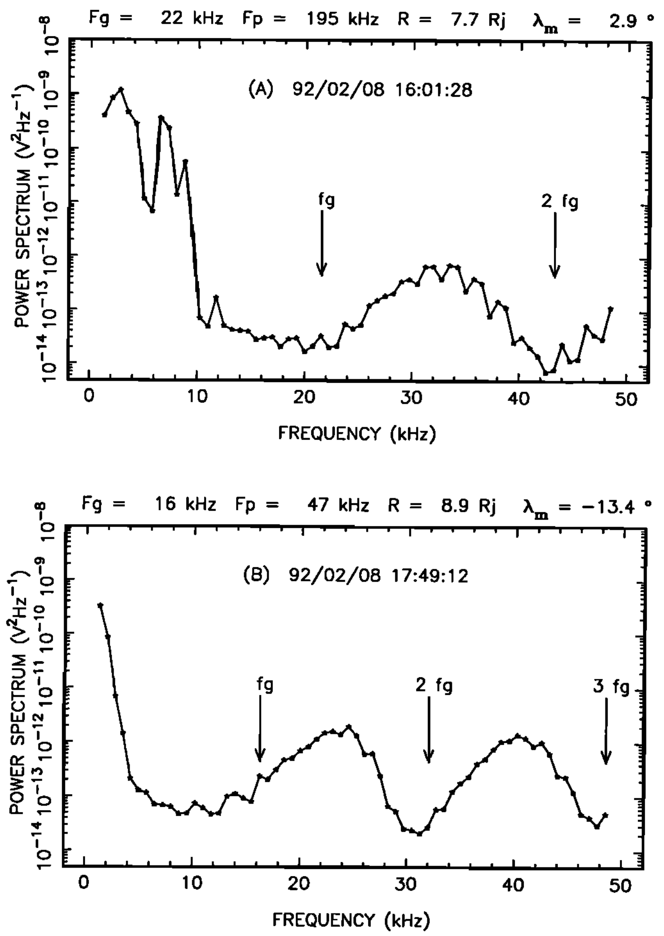

Fig. 2. Typical spectra in (*a*) the torus and (*b*) its outer fringe. The arrows indicate harmonics of the electron gyrofrequency f_g. The labels correspond to radial distance to Jupiter (R), magnetic latitude (λ_m), and plasma frequency (f_p).

region, except near equator crossing, these bursts have an upper cutoff near $f_g/2$, shown as a dashed line in the lower panel (see section 4.2).

Apart from the upper hybrid noise and the bursty emissions, the most conspicuous features of the spectrum are smooth banded noise between consecutive harmonics of the gyrofrequency, below the plasma frequency. This paper focuses on these bands, which can only be observed properly with the low-frequency receiver because of its high resolution in frequency.

We will concentrate on the torus crossing; farther away from the planet, the radio experiment was generally set in a mode using cross correlations of the spin-plane dipole and the spin axis monopole antenna, which heavily complicates the interpretation.

Figure 2 shows typical spectra (i.e., vertical cuts of Figure 1), obtained respectively (*a*) in the densest region explored by Ulysses and (*b*) in the outer fringe of the torus. Each spectrum corresponds to a linear frequency sweep of the receiver lasting 128 s, and each plotted data point is the average of four successive measurements acquired at each frequency within a 2-s step. The spectra have well-defined minima near harmonics of the gyrofrequency, with smooth maxima between them. In the examples shown the maxima occur at the center of the intraharmonic bands, but this is not always so. There is also a small-scale modulation due to the spacecraft rotation, which changes the orientation of the antenna with respect to the magnetic field (during half a spin period, the receiver frequency sweeps by ~2 kHz).

In general, the maximum spectral density is rather small: $\sim 10^{-12}$ V^2 Hz^{-1} in the middle of the harmonic bands and varies very smoothly in time and frequency. This prompted us to investigate the simplest interpretation: that it might be due to quasi-thermal fluctuations in Bernstein modes. Since these modes are electrostatic waves propagating perpendicular to the magnetic field, their reception should be a function of the antenna orientation, and the observed spin modulation is an important clue to their identification.

2.2. *Spin Modulation*

Since the spin modulation is not clearly seen on the concise presentation of Figure 2 (because of the averaging), we have plotted in Figure 3 the unaveraged spectral density as a function of time for each frequency sweep, together with the angle θ between the antenna and the magnetic field **B** calculated from the magnetometer data [*Balogh et al.*, 1992].

In the high-frequency part of the intraharmonic bands, where the modulation is largest, the spectral density is maximum when the antenna is perpendicular to **B** and varies roughly as $\sin^2 \theta$ (with small superimposed variations which may be due in part to small-scale plasma or magnetic variations). This is just the behavior expected for waves polarized perpendicular to **B**. However, the modulation depth decreases with frequency within the bands and becomes very small near $\theta \sim \pi/2$ at a normalized frequency $f/f_g \sim 1.3$–1.6 (depending on the location in the torus) in the first band, and at larger values of $f/f_g - n$ in the second ($n = 2$) band. In the low-frequency part of the bands the modulation is completely different: the signal has a broad minimum when the antenna is perpendicular to **B** (with a secondary minimum at $\theta \approx 0$), and the modulation depth is smaller. It may also be noted that the first minimum of the spectral shape is slightly below the first harmonic $f/f_g = 1$, whereas the following ones are near $f/f_g = n$ within a few percent. We shall return to this point in section 3.4.3. Other spectra acquired in the torus show a similar qualitative behavior.

At large distances from the equatorial plane and farther out from Jupiter the magnetic field makes a smaller angle with the spin axis, so that θ varies much less as the spacecraft spins. So does the spectral density, as can be seen in Figure 2*b*, where the modulation is very small and difficult to analyze.

2.3. *Magnetic Equator Crossing*

During the few minutes when the spacecraft is within roughly ±2° magnetic latitude the level is strongly enhanced (often saturating the receiver at a level $\sim 10^{-9}$ V^2 Hz^{-1}) and rather bursty near $3f_g/2$, with a typical bandwidth $\Delta f/f \sim 0.1$–0.3; data from the high-frequency receiver indicate that higher harmonics are also present (see Figure 1 near 1616 UT).

Figure 4 shows three successive frequency sweeps acquired just before the magnetic equator crossing. Although it is more difficult to study because of the partial saturation, the spin modulation appears to have the same behavior as farther from the equator. As the spacecraft approaches the magnetic equator, the spectral density increases, culminating at $\lambda_m \approx 0°$. The corresponding spectrum (not shown because it is heavily saturated) appears to have a spectral

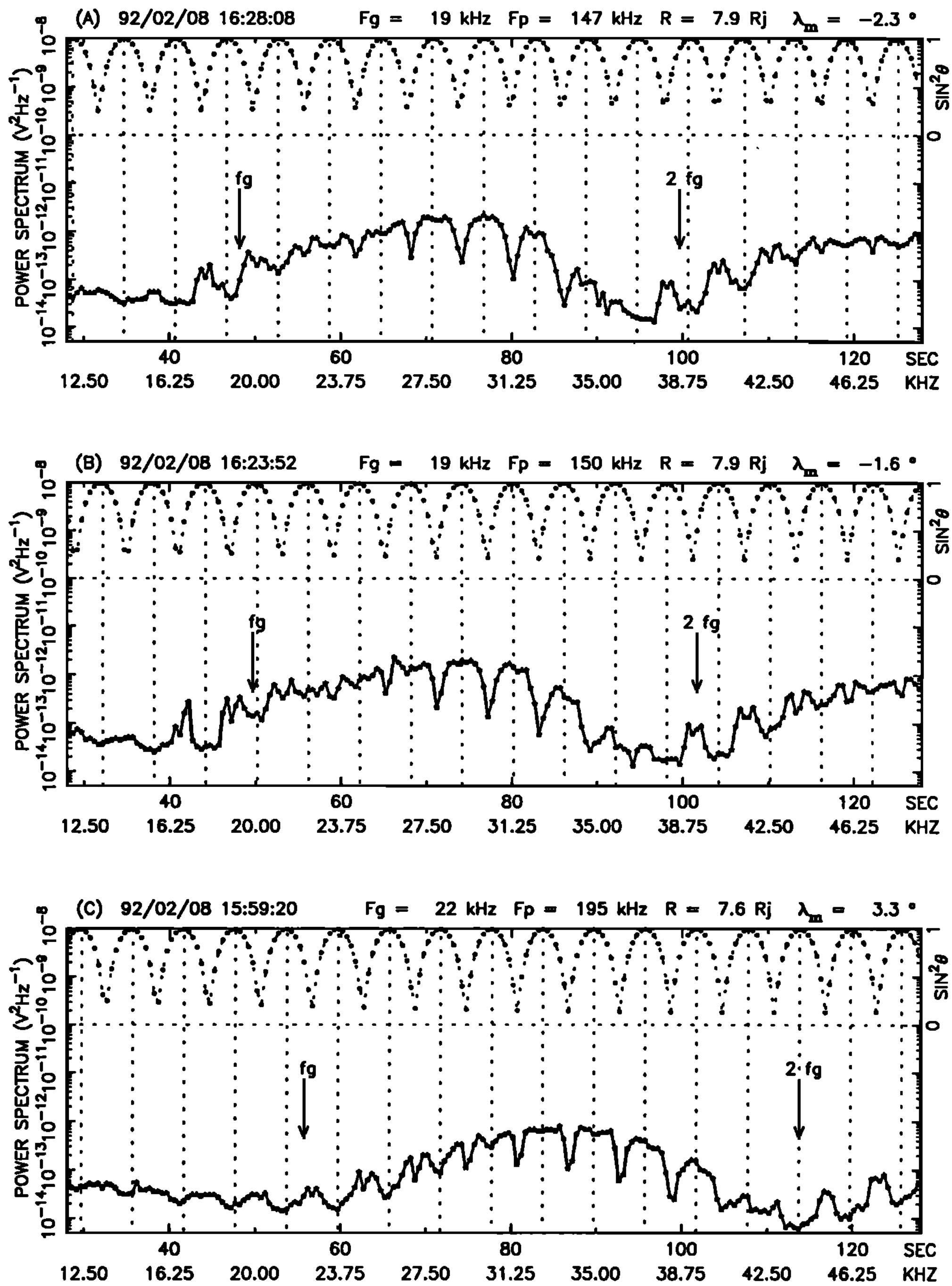

Fig. 3. Spectral power density as a function of time (seconds counted from the beginning of the frequency sweep) for three frequency sweeps within the torus. Corresponding frequencies (in kilohertz) are indicated at the bottom. The arrows indicate harmonics of the electron gyrofrequency f_g. The angle θ between the antenna and the magnetic field, computed using the magnetometer data (courtesy of A. Balogh) is plotted as $\sin^2 \theta$ at the top. Dashed vertical lines indicate times when $\theta = \pi/2$. The values of the parameters indicated above each panel were measured half way through the frequency sweep.

shape and spin modulation different from the other spectra, suggesting an important change in the wave vector or the ambient magnetic field.

Similar high-intensity "$(n + 1/2)f_g$" emissions confined to within a few degrees of the magnetic equator have been observed in the magnetospheres of the Earth [see *Kennel et al.*, 1970] and other planets. There is a large body of literature on their interpretation in terms of various plasma instabilities (see *Kennel and Ashour-Abdalla* [1982] for a review). Our observations in the magnetic equatorial plane are most probably due to a plasma instability, and Figure 4 presumably illustrates the noise increase associated with an increase of non-Maxwellian features in the distribution function, as instability is approached. However, the identification of the instability would be difficult, since there are no simultaneous measurements of the electron distribution, and we concentrate here on the weak emissions observed farther from the equator.

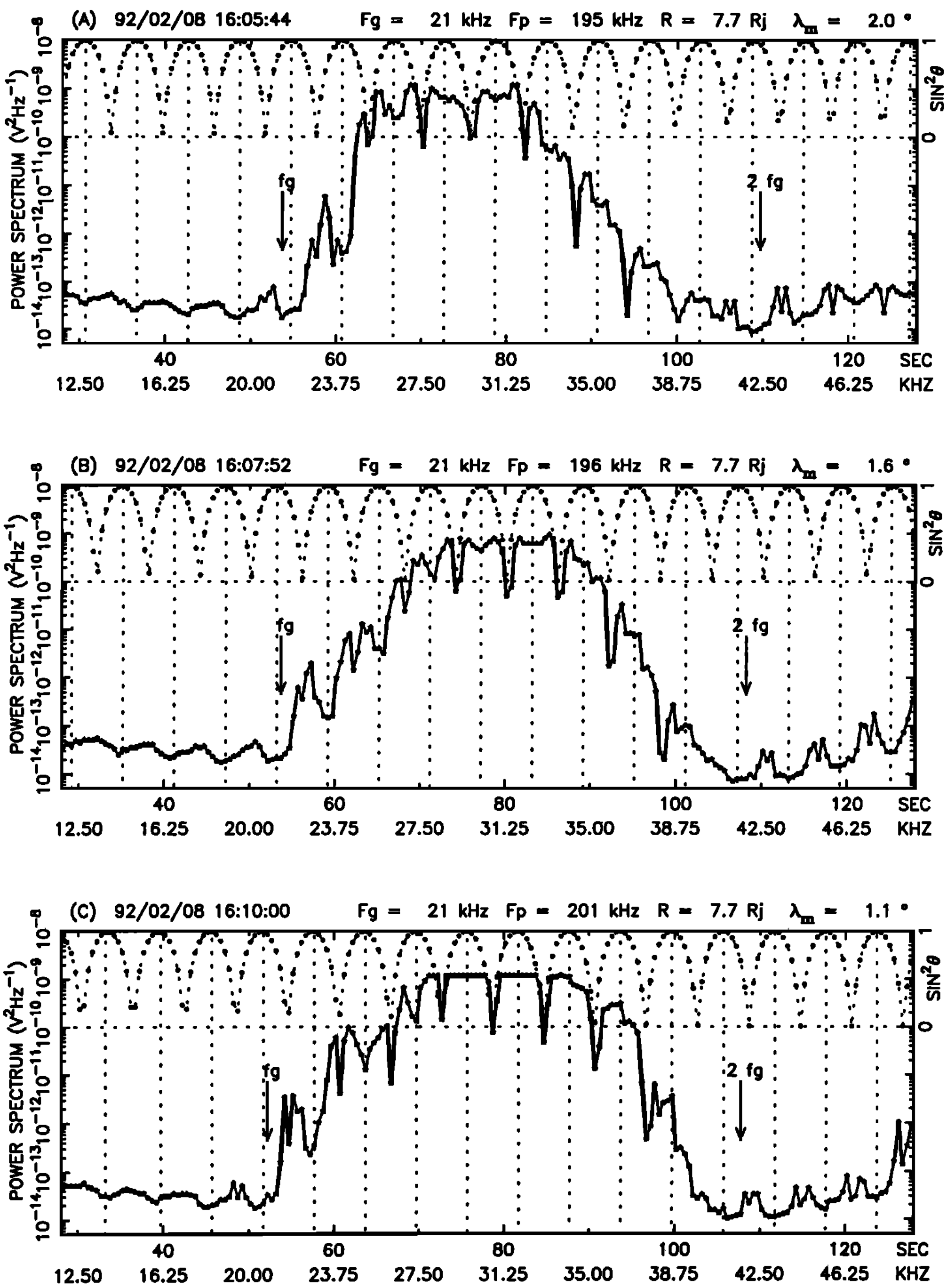

Fig. 4. Three consecutive frequency sweeps showing the power spectral density just before the magnetic equatorial plane crossing. The labels are the same as in Figure 3.

3. THEORY

In order to interpret the observations in terms of Bernstein waves we have to address two points. First, since these modes are longitudinal and propagate perpendicular to the magnetic field, one might expect naively that the amplitude should always be maximum when the antenna is perpendicular to **B**. So, why does the apparent polarization change in the lower frequency part of the intraharmonic bands? A clue [*Meyer-Vernet and Perche*, 1989] might be that when the antenna is a filamental dipole of length L longer than the relevant wavelengths (i.e., $kL \gg 1$), its response modifies the apparent polarization of longitudinal waves. This is because the antenna is mostly sensitive to waves whose wavelengths along the antenna are of the order of its length. In order to have a projection $\sim 1/L$ with a modulus $\gg 1/L$, the vector **k** should make a large angle with the antenna direction; since $\mathbf{E} \parallel \mathbf{k}$, this produces an apparent polarization perpendicular to the expected one. We shall put this crude argument on a quantitative basis for the specific case of Bernstein waves received by the URAP antenna. We will also estimate the noise theoretical level.

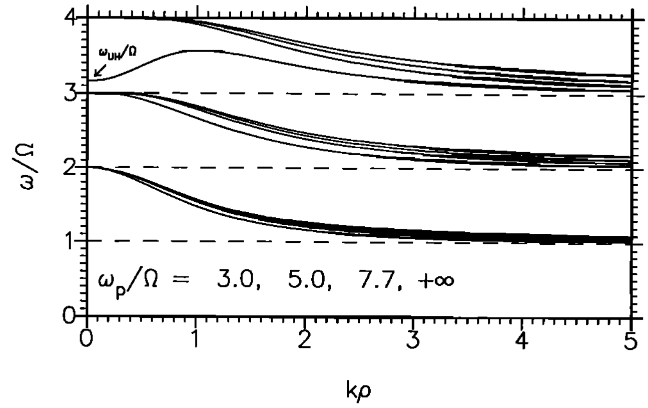

Fig. 5. Bernstein modes ($k = k_\perp$) drawn as ω/Ω versus $k\rho$ for different values of the parameter ω_p/Ω increasing from left to right. (The case $\omega_p/\Omega = 7.7$ corresponds to the spectrum of Figure 3*a*, and its first harmonic band is nearly identical to the limiting curve $\omega_p/\Omega \to \infty$ shown here for comparison.) The results correspond to a Maxwellian plasma but are not significantly changed by a very small proportion of suprathermal electrons.

3.1. *Bernstein Waves*

Bernstein waves [*Bernstein*, 1958] are an infinite set of undamped longitudinal modes propagating across the magnetic field, between harmonics of the electron gyrofrequency, in a Maxwellian electron plasma described by the Vlasov equation. In this ideal case the dispersion equation has the implicit form:

$$\varepsilon = 0 = 1 - \frac{\omega_p^2}{\Omega^2}\frac{e^{-k^2\rho^2}}{k^2\rho^2}\sum_{n=-\infty}^{+\infty}\frac{nI_n(k^2\rho^2)}{\omega/\Omega - n} \tag{1}$$

where I_n is a modified Bessel function of the first kind, $\omega_p = 2\pi f_p$ and $\Omega = 2\pi f_g$ are respectively the electron (angular) plasma frequency and gyrofrequency, and

$$\rho = (k_B T/m_e)^{1/2}/\Omega \tag{2}$$

the thermal electron gyroradius; here m_e and T denote the electron mass and temperature and k_B is Boltzmann's constant. This is valid for low-β plasmas, in order that transverse and longitudinal modes decouple, and frequencies sufficiently high so that ion motions can be neglected. In the part of the torus explored by Ulysses we find indeed

$$\beta = 2\mu_0 n_e k_B T/B^2 \sim 3 \times 10^{-3} \tag{3}$$

for electrons near the magnetic equator, and still smaller values at larger latitudes.

A Bernstein mode propagates in each gyroharmonic band $n < \omega/\Omega < (n + 1)$, as illustrated in Figure 5, which shows the lowest bands for several values of the ratio ω_p/Ω. In those bands the solution is nearly independent of ω_p when $\omega_p/\Omega \gg 1$ (except for $k\rho \gg 1$), as may be seen from (1) since the second term is in this case much larger than 1, so that ω_p factorizes out of the equation. This condition is satisfied in a significant part of the torus explored by Ulysses.

In particular for the first intraharmonic band, one has $k\rho \to \infty$ for $\omega/\Omega \to 1$, $k\rho \sim 1$ in the middle of the band, and $k\rho \to 0$ for $\omega/\Omega \to 2$. The results are similar in the second band, k being somewhat larger for a given position within the band. This is so up to the upper hybrid frequency, k regularly increasing with the order of the band. (For larger frequencies there is a qualitative change of behavior: there are two solutions for a given frequency, merging at the so-called f_Q frequencies, and the mode fills only a fraction of the band.)

These results correspond to a Maxwellian distribution. In the region of the torus explored by Ulysses, at ~8 R_J from Jupiter, there is a very small concentration of suprathermal electrons (~ a few percent [*Sittler and Strobel*, 1987]). This does not change significantly the solutions of the dispersion equation calculated here, so that we may use (1), with the parameters of the main (cold) population. This would not be so in the presence of a larger proportion of hot electrons (see, for example, *Belmont* [1981]). One may also note that if the cold population is anisotropic, then (1) still holds, but the gyroradius involves the thermal velocity normal to the magnetic field (see, for example, *Kennel and Ashour-Abdalla* [1982]).

These undamped modes propagate perpendicular to the magnetic field ($k_\parallel = 0$). For oblique propagation the dispersion equation has an imaginary part and the waves are damped; however, if $|k_\parallel| \ll k_\perp$, they remain rather similar to Bernstein modes. In the extreme case of parallel propagation ($k_\perp = 0$) the dispersion equation reduces to that without a magnetic field.

3.2. *Bernstein Waves as Seen With a Dipole Antenna*

Consider a dipole antenna parallel to the x axis, immersed in a fluctuating electric field whose autocorrelation spectrum in this direction is $E_x^2(\mathbf{k}, \omega)$. The voltage power spectrum at the antenna terminals is

$$V_\omega^2 = \frac{2}{(2\pi)^3}\int d^3k|J(\mathbf{k})|^2E_x^2(\mathbf{k}, \omega) \tag{4}$$

where $J(\mathbf{k})$ is the Fourier transform of the current distribution on the antenna. This expression conforms to the usual definition of the spectral density, which is in units of V^2 Hz^{-1} since $\int_0^\infty V_\omega^2\, d(\omega/2\pi) = \langle V^2\rangle$; in the case of thermal equilibrium, it is related to the antenna resistance R by the Nyquist relation $V_\omega^2 = 4k_BTR$ [see *Meyer-Vernet and Perche*, 1989].

3.2.1. *Filamental dipole.* For a dipole made of two thin filaments, each of length L much larger than their radius or width, one has

$$J(\mathbf{k}) = 4\,\frac{\sin^2(k_xL/2)}{k_x^2L} \tag{5}$$

This assumes that the current distribution is triangular, decreasing linearly with distance along each arm, or equivalently that the measured voltage is the difference between the voltages averaged over each arm; this requires at least the condition: $\omega L/c \ll 1$, c being the velocity of light (see, for example, *Meyer et al.* [1974]).

To calculate the antenna response to Bernstein waves, we consider a longitudinal ($\mathbf{E} \parallel \mathbf{k}$) and gyrotropic electric field, being essentially in a plane perpendicular to the static magnetic field ($|k_\parallel| \ll k_\perp$). The projected spectrum is $E_x^2(\mathbf{k}, \omega) = E^2(k_\perp, k_\parallel, \omega)\cos^2\alpha$, where α is the angle between $\mathbf{k}$ and the antenna direction. Let θ be the angle between the antenna and the ambient magnetic field (modulo π), and ϕ the azimuthal angle of $\mathbf{k}$ in a plane perpendicular to $\mathbf{B}$. We have $\cos\alpha \approx \sin\theta\cos\phi$, if $|k_\parallel|/k_\perp \ll \tan\theta$. The integral (4) may thus be written

$$V_\omega^2 \approx \frac{2}{(2\pi)^3}\int_0^\infty k_\perp\, dk_\perp \int_{-\infty}^{+\infty} dk_\parallel E^2(k_\perp, k_\parallel, \omega)$$

$$\cdot \int_0^{2\pi} d\phi\, \frac{16\sin^4(k_\perp \sin\theta\cos\phi L/2)}{k_\perp^4 L^2 \sin^2\theta\cos^2\phi}$$

$$\approx \frac{1}{4\pi^2}\int_0^\infty \frac{dk_\perp}{k_\perp}\int_{-\infty}^{+\infty} dk_\parallel E^2(k_\perp, k_\parallel, \omega) F_\perp(k_\perp L\sin\theta) \tag{6}$$

where we have put $u = k_\perp L \sin\theta$, $t = u\cos\phi$, and the antenna response function is defined as

$$F_\perp(u) = \frac{64}{\pi}\int_0^u dt\, \frac{\sin^4(t/2)}{t^2(u^2-t^2)^{1/2}} \tag{7}$$

(as already said, this assumes that the electric field spectrum is negligible for $|k_\parallel| \not\ll k_\perp$, and that θ is not too close to zero, namely, $\tan\theta \gg |k_\parallel|/k_\perp$). The response can also be written in the following equivalent form:

$$F_\perp(u) = \frac{8}{u}\Big[2\int_0^u dt\, J_0(t) - \int_0^{2u} dt\, J_0(t) + J_1(2u) - 2J_1(u)\Big] \tag{8}$$

(the integral of J_0 is tabulated by *Abramowitz and Stegun* [1970]).

This function is plotted in Figure 6. Apart from a factor u^2, it has been calculated by [*Sentman*, 1982] for an antenna perpendicular to $\mathbf{B}$ (see Figure 11 of that paper, in which θ denotes the angle $[\mathbf{k}, \mathbf{B}]$ which is roughly equal to $\pi/2$ for Bernstein waves). To gain an insight into its behavior, let us obtain analytical approximations for small or large u. For small u we expand the sine in a power series and integrate the first two terms. For large u we obtain the leading term of the asymptotic expansion by noting that the bracket in (8) tends to 1 when $u \to \infty$, since $J_1(u) \to 0$ and $\int_0^\infty J_n(x)\,dx \equiv 1$. Then

$$F_\perp(u) \sim u^2(1 - u^2/8) \qquad (u < 1) \tag{9}$$

$$F_\perp(u) \sim 8/u \qquad (u \gg 1) \tag{10}$$

Up to $u = k_\perp L\sin\theta \sim 1$, the response function is nearly equal to u^2: the antenna behaves as a short dipole. For larger values of u the response exhibits a maximum and ultimately decreases with u. This should especially reduce the apparent spectral density of Bernstein waves near the lower end of the intraharmonic bands, where $k_\perp \to \infty$.

Let us now calculate the apparent polarization. We shall see that the fluctuation spectrum $E^2(k_\perp, k_\parallel, \omega)$ of Bernstein waves, for the bands below ω_{UH}, is roughly a delta function in $k_\perp$, involving the solution of the dispersion equation at the frequency ω. In this case, one sees from (6) that the spectral density varies with the angle θ between the antenna and $\mathbf{B}$ as

$$V_\omega^2 \propto F_\perp(k_\perp L\sin\theta)$$

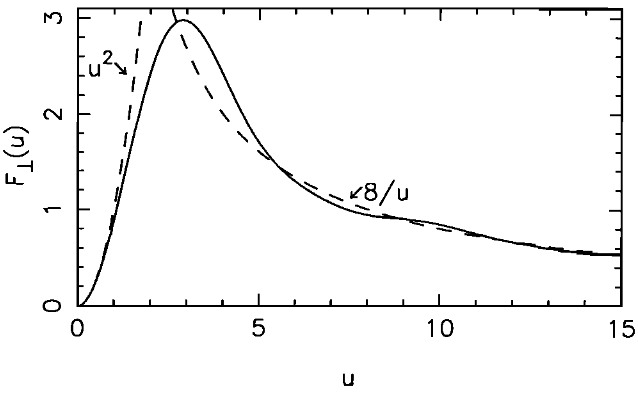

Fig. 6. Graph of the function $F_\perp(u)$ defined in (7), which determines the spin modulation: the spectral density varies with the angle θ between the antenna and the magnetic field as $F_\perp(k_\perp L \sin\theta)$.

From (9) and (10) we have in particular:

$$V_\omega^2 \propto \sin^2\theta \qquad k_\perp L\sin\theta \le 1 \tag{11}$$

$$V_\omega^2 \propto 1/\sin\theta \qquad k_\perp L\sin\theta \gg 1 \tag{12}$$

Hence for small values of $k_\perp L$ the noise varies as $\sin^2\theta$, being maximum when the antenna is perpendicular to $\mathbf{B}$, in agreement with the naive reasoning. On the contrary when $k_\perp L$ is large the noise level has a minimum at $\theta = \pi/2$, with another minimum at $\theta = 0$ (since if $k_\perp L\sin\theta \to 0$, (11) holds). For Bernstein waves this counterintuitive behavior should take place in the lower part of the intraharmonic bands, where $k_\perp$ is large. Figure 7 shows examples of the predicted spin modulation for different values of $k_\perp L$, in the ideal case when the magnetic field is in the antenna spin plane. Note that in general, $\mathbf{B}$ makes a finite angle s with this plane, so that $\sin\theta$ varies only between $\sin s$ and 1 during the spacecraft rotation; that is, θ is never exactly 0 or π.

The transition between the two regimes of spin modulation occurs at the extremum of the function $F_\perp(u)$, which takes place at $u \approx 3$; that is,

$$k_\perp L \approx 3 \tag{13}$$

Since $k_\perp\rho$ and ω/Ω are related through Bernstein's dispersion equation, this opens an interesting possibility: from the frequency at which the behavior of the spin modulation changes, one can deduce the gyroradius and thus the electron temperature. If $\omega_p^2/\Omega^2 \gg 1$, the result in the first intraharmonic bands does not depend on ω_p.

These results are relevant for a filamental dipole antenna, like that used by the URAP experiment aboard Ulysses. However, a number of experiments use dipoles made up of two small spheres; such was the case on GEOS or ISEE 1. What are the antenna response and the modulation in that geometry?

3.2.2. *Double-sphere antenna.* With two small spheres separated by L along the x axis the Fourier transform of the current distribution is

$$J(\mathbf{k}) = -2i\,\frac{\sin(k_x L/2)}{k_x} \tag{14}$$

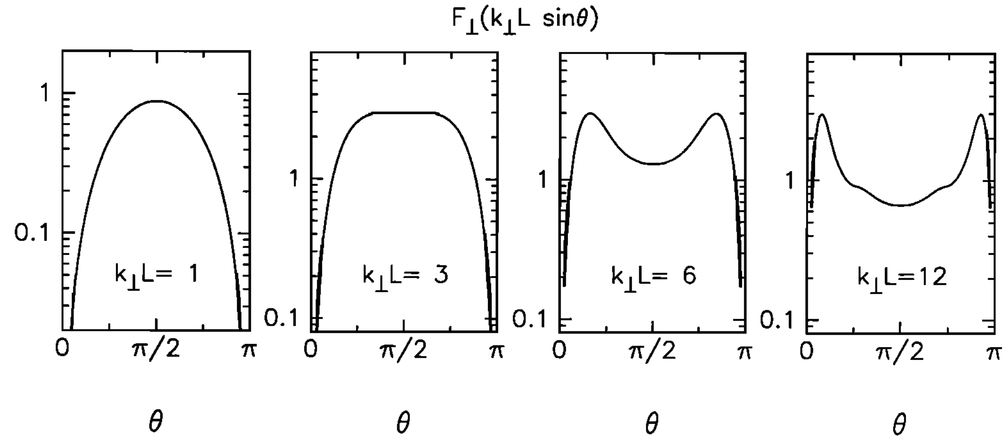

Fig. 7. Graph of $F_\perp(k_\perp L \sin\theta)$ as a function of the angle θ between the antenna and the magnetic field for different values of $k_\perp L$. The predicted spectral density $V_\omega^2 \propto F_\perp$ varies as $\sin^2\theta$ for $k_\perp L \le 1$ but has a minimum at $\theta = \pi/2$ for $k_\perp L > 3$ (the other minimum at $\theta = 0$, modulo π, should be observed only if very small values of θ are actually encountered). From Bernstein's dispersion equation, small (or large) $k_\perp$ correspond respectively to the high- (or low) frequency part of the harmonic bands.

Substituting this expression into (4) gives the antenna response function for Bernstein waves:

$$F_\perp(u) = \frac{16}{\pi}\int_0^u dt\,\frac{\sin^2(t/2)}{(u^2-t^2)^{1/2}} \tag{15}$$

This can be trivially transformed into tabulated integrals [*Gradshteyn and Ryzhik*, 1980], and we find

$$F_\perp(u) = 4[1 - J_0(u)] \tag{16}$$

For small or large u this gives

$$F_\perp(u) \sim u^2(1 - u^2/16) \qquad (u < 1) \tag{17}$$

$$F_\perp(u) \sim 4 \qquad (u \gg 1) \tag{18}$$

As expected, a short double-sphere dipole ($u < 1$) behaves like a filamental one. However for $k_\perp L \sin\theta \gg 1$ the response is larger than with a filament and independent of $k_\perp L \sin\theta$. Therefore with this kind of antenna the noise becomes independent of the antenna orientation for large $k_\perp L$ (except for θ small enough to make $k_\perp L \sin\theta \ll 1$, for which one recovers the $\sin^2\theta$ variation). It does not exhibit the change in the apparent direction of polarization found for a filament.

We note that a similar difference in the response functions of both antenna geometries occurs when the fluctuation spectrum is isotropic instead of gyrotropic (see, for example, *Meyer-Vernet* [1979]).

3.3. *Quasi-Thermal Noise in Bernstein Waves*

Sentman [1982] calculated the quasi-thermal noise in Bernstein waves, for an antenna perpendicular to the magnetic field, in a plasma with an electron distribution made of two Maxwellians with $n_h/n_c \ll 1$ and $T_h/T_c \gg 1$. This section is based on his analytical results, which we reformulate here for consistency with section 3.2 and extend for an arbitrary antenna orientation.

Though space plasmas are generally not in thermal equilibrium, modeling distributions with sums of Maxwellians is a traditional starting point, which was indeed used to present the particle measurements made aboard Voyager in the Io torus [*Sittler and Strobel*, 1987].

True Bernstein waves ($k_\parallel = 0$) are undamped, and we assume that the major contribution to the spectrum comes from waves whose damping is very small. Their contribution to the spectral density may be obtained from the electric field autocorrelation spectrum in the vicinity of a nearly real solution of the dispersion equation (i.e., $\varepsilon_r(\mathbf{k}, \omega) = 0$),

$$E^2(\mathbf{k}, \omega) \approx 2\pi\,\frac{k_B T_h}{\omega\varepsilon_0}\,\delta(\varepsilon_r)$$

To obtain a rough estimate below ω_{UH}, one may take this amplitude for $k_\perp$ equal to the (unique) solution of the Bernstein dispersion equation (1) at the frequency ω, and $k_\parallel$ in the range $|k_\parallel| \le \Delta k_\parallel \ll k_\perp$; that is,

$$E^2(k_\perp, k_\parallel, \omega) \approx 2\pi\,\frac{k_B T_h}{\omega\varepsilon_0}\,\frac{\delta(k - k_\perp)}{|\partial\varepsilon_r/\partial k_\perp|_{k_\parallel = 0}} \quad (|k_\parallel| \le \Delta k_\parallel) \tag{19}$$

where the derivative is taken at the solution k of Bernstein's dispersion equation.

The width $\Delta k_\parallel$ corresponds to the maximum value of $|k_\parallel|$ for which the hot population still makes the dominant contribution to the imaginary part of ε. For the cold (c) or hot (h) populations respectively the contributions vary as

$$\varepsilon_{i(c,h)} \propto \frac{n_{c,h}}{T_{c,h}^{3/2}}\,e^{-k_\perp^2\rho_{c,h}^2}\,I_n(k_\perp^2\rho_{c,h}^2)\,e^{-(\omega/\Omega - n)^2/2k_\parallel^2\rho_{c,h}^2} \tag{20}$$

where n labels the dominant term, which is determined by the order of the band in question. Approximating the hot exponential term by 1, using the asymptotic expansions of the Bessel functions (which hold for $k_\perp^2\rho_{c,h}^2 \gg 1$), and noting that the gyroradii $\rho_{c,h} \propto T_{c,h}^{1/2}$, one obtains

$$\Delta k_\parallel\rho_c \sim \frac{\min|\omega/\Omega - n|}{2^{1/2}}\left[\ln\left(\frac{n_c T_h^2}{n_h T_c^2}\right)\right]^{-1/2} \tag{21}$$

Inserting (19) into (6) and integrating gives

$$V_\omega^2 \approx \frac{F_\perp(k_\perp L \sin\theta)}{\pi\varepsilon_0}\left[\frac{(\Omega/\omega)\Delta k_\parallel/k_\perp}{|\partial\varepsilon_r/\partial k_\perp\rho_c|_{k_\parallel=0}}\right]\frac{k_B T_h}{\Omega\rho_c} \quad (22)$$

where $k_\perp$ denotes the solution of Bernstein's dispersion equation for the (angular) frequency ω. Apart from the arbitrary antenna orientation, and considering our definition of the gyroradius (equation (2) with $T = T_c$), this is essentially equivalent to (39) of [*Sentman*, 1982], although not to his (41), owing to his different definition of the relevant power spectrum. The term in brackets is a weak function of the plasma parameters. For an order-of-magnitude estimate in the outer torus we take $n_h/n_c \sim 10^{-2}$, $T_h/T_c \sim 30$ [*Sittler and Strobel*, 1987], which gives $\Delta k_\parallel \rho_c \sim 0.1$ near the center of the intraharmonic bands (where it is largest); changing these parameters by as much as a factor of 10 does not significantly change the result. The other factors of the term in brackets should have an order of magnitude of 1 near the center of the first intraharmonic bands (where $k_\perp\rho_c \sim 1$). This yields

$$V_\omega^2 \sim 1.3\times 10^{-17} F_\perp(k_\perp L \sin\theta)(T_h/T_c^{1/2}) \quad (23)$$

In particular, substituting $k_\perp\rho_c \sim 1$ and $\Omega = 2\pi f_g$, we have for $L \sin\theta \le \rho_c$ (antenna length smaller than the cold gyroradius):

$$V_\omega^2 \sim 0.1 \times L^2 \sin^2\theta \, \frac{k_B T_h}{\pi\varepsilon_0\Omega\rho_c^3}$$

$$\sim 3\times 10^{-23}\, L^2 \sin^2\theta \, \frac{T_h f_g^2}{T_c^{3/2}} \quad (24)$$

and for $L \sin\theta \gg \rho_c$ (antenna length much larger than the cold gyroradius):

$$V_\omega^2 \sim 6\times 10^{-14}\,\frac{T_h}{f_g L \sin\theta} \quad (25)$$

(in V^2 Hz^{-1}; the temperatures are in kelvin and the gyrofrequency in hertz).

It may be interesting to note that (when f and f_P have similar orders of magnitudes) (24) can be obtained "on the back of an envelope" as follows. The mean electrostatic energy of quasi-thermal fluctuations per unit volume $\varepsilon_0\langle E^2\rangle/2$ is equal to $k_B T_h$ per mode **k**, in a volume V_k of k space defined by $k_\perp \sim 1/\rho_c$ and $|k_\parallel| \le \Delta k_\parallel \sim 0.1/\rho_c$; that is, $V_k \sim 0.1 \times 2\pi/\rho_c^3$. With a bandwidth $\sim f_g$ this gives

$$E_\omega^2 \sim \langle E^2\rangle/f_g \sim 2\mathcal{N} k_B T_h/\varepsilon_0 f_g$$

where $\mathcal{N}$ is the number of modes per unit volume, which is related to the volume in k space by $\mathcal{N} = V_k/(2\pi)^3$. Since the voltage power spectrum is $V_\omega^2 \approx L^2 E_\omega^2$ for a short antenna, this yields (24).

These results are order-of-magnitude estimates for the center of the first intraharmonic bands. A precise calculation would require numerical computations as performed by [*Sentman*, 1982], with, however, further difficulties discussed below.

3.4. *Discussion*

3.4.1. *Electron distribution function.* Modeling the electron distribution by a sum of two Maxwellians is a rather rough approximation in the Io torus [*Scudder and Sittler*, 1981]. This is far from being innocuous here, because the spectral density in Bernstein waves (which have $k_\parallel \to 0$ and resonate with electrons of parallel velocity $\sim(\omega - n\Omega)/k_\parallel$) is very sensitive to the hot electron distribution. Non-maxwellian features of the hot electrons, even small, may significantly increase the spectral density [*Sentman*, 1982].

On the other hand, the solution $k_\perp$ of the dispersion equation is mainly determined by the main (cold) population and not significantly affected by a very small proportion of hot electrons. Hence the spin modulation, which only depends on $k_\perp L$ (provided that $k_\parallel \ll k_\perp$), should not be very sensitive to non-Maxwellian features of these hot electrons.

We thus expect that the quasi-thermal noise should provide a reliable measurement of T_c (from the observed spin modulation) but a more hazardous measurement of T_h (from the absolute spectral density). This is reminiscent of what is known in the absence of a magnetic field [*Chateau and Meyer-Vernet*, 1991] and has a similar origin: the cold electron measurement rests on a quantity that depends on low-order moments of the distribution function, whereas the measurement of hot electrons depends directly on the distribution function or its derivative. In the first case the details are smoothed out in the integration process, whereas they show up in the second case.

3.4.2. *Antenna impedance.* The calculated spectral density represents a noise level at the antenna ports, whereas the measurements are made at the receiver ports. Both quantities are equal when the antenna impedance is much smaller than that of the receiver which is in practice that of the base capacitance, known from calibration data.

In the present case the antenna impedance is not easy to calculate because the usual simplifying approximations (see, for example, *Balmain* [1964], *Meyer and Vernet* [1974], and *Nakatani and Kuehl* [1976]) break down. However, we note that since ω, $\Omega \ll \omega_p$, the antenna impedance is expected to be rather small. When the spacecraft potential is negative, an important contribution to the impedance stems from the ion sheath surrounding the antenna; this contribution, however, is not sufficient to make the voltage at the receiver ports different in order of magnitude from that at the antenna ports. Hence for the present order-of-magnitude estimates we will assume that the signal levels at the receiver and antenna ports are approximately equal.

3.4.3. *Doppler shift.* The calculation assumes that the antenna is at rest in the plasma frame. In practice, however, there is a relative motion of velocity **V**, so that for each **k** in the spectral density integral, the angular frequency ω must be replaced by the Doppler-shifted value $\omega - \mathbf{k}\cdot\mathbf{V}$.

In the torus the relative velocity may be assumed to be of the order of magnitude of the corotation velocity. At low latitudes and typical distances corresponding to our data ($R \sim 8\, R_J$) this gives $V \approx 10^5$ m/s. At the frequency where the apparent polarization changes we have $k_\perp = 3/L$. Putting $L = 35$ m and ω at receiver midband ($f \sim 25$ kHz), we get for the relative Doppler shift near the frequency of apparent polarization change:

$$|\Delta\omega|/\omega \le k_\perp V/\omega \sim 0.05 \quad (26)$$

This suggests that the resulting shift of that frequency should be rather small.

Near the lower end of the intraharmonic bands, where $k_\perp$ is large, one expects from (26) a larger effect. This should especially change the spectral shape near the first harmonic $\omega \sim \Omega$ since the spectrum near higher harmonics depends on both very large (just above $n\Omega$) and very small (just below $n\Omega$) values of $k_\perp$. Roughly speaking, since the antenna response decreases for large $k_\perp$, the wave vectors such that $\mathbf{k} \cdot \mathbf{V} < 0$ play a dominant role since they give a larger shifted frequency and thus decrease the solution $k_\perp$ of the dispersion equation. Thus one expects that the spectrum minimum occurring at an effective frequency equal to the gyrofrequency will correspond to a smaller real frequency, so that the minimum at the lower end of the first band should be shifted slightly below f_g. On the other hand, the change should be smaller near the upper end of the bands where $k_\perp \to 0$.

This effect might also introduce a small additional spin modulation, produced by the change in the orientation of the antenna with respect to the velocity direction.

3.4.4. *Other contributions to the spectral density.* The contribution of Bernstein waves tends to zero at gyroharmonics, where one should essentially see thermal fluctuations and the shot noise due to particle impacts or emission at the antenna surface. The latter contribution gives an approximate f^{-2} noise, which depends on the spacecraft potential when it is negative; it is expected to be rather small above the gyrofrequency when $\omega_p \gg \Omega$, owing to the small antenna impedance.

To get a rough estimate of the thermal noise, one may use the results calculated below the plasma frequency in the absence of a magnetic field [see *Meyer-Vernet and Perche*, 1989], which should hold in order of magnitude since the gyroradius is much larger than the Debye length L_D. In the case $L \gg L_D$ relevant here it has the approximate analytical expression:

$$V_{\omega T}^2 \sim \left(\frac{2}{\pi}\right)^{1/2} \frac{k_B T_c}{\varepsilon_0 L f_p} \sim 3 \times 10^{-13} \frac{T_c}{L f_p} \qquad (27)$$

(in V^2 Hz^{-1}; T_c is in kelvins, f_p in hertz, and L in meters).

4. APPLICATION TO ULYSSES OBSERVATIONS

4.1. *Spin Modulation: Measuring the Cold Temperature*

The observed spin modulation agrees rather well with the theory throughout the data, varying roughly as $\sin^2\theta$ in the upper part of the intraharmonic bands, and exhibiting the predicted change of shape in the lower part, with a minimum at $\theta = \pi/2$ and a smaller modulation depth; in that frequency range it also exhibits the other predicted minimum near $\sin\theta = 0$ (in practice, due to the finite angle between the antenna spin plane and $\mathbf{B}$, $\sin\theta$ does not go through very small values, so that this latter minimum appears as a secondary one). This agreement suggests that other sources of spin modulation play a smaller role. Hence such complications as the bulk velocity, the finite antenna impedance, a possibly more complicated current distribution on the antenna, or the finite value of $k_\parallel$ seem to be secondary effects.

The spin modulation shape predicted for $k_\perp L > 3$ is generally observed over the whole first half of the second band, whereas it is only observed in a smaller fraction of the first band; this agrees with the fact that the solutions $\omega(k_\perp)$ of Bernstein's dispersion equation increase in relative position within a band as the order of the band increases (see Figure 5).

To get the electron temperature from the data, one has to determine the frequency f_m at which the sense of the spin modulation (near $\theta = \pi/2$) changes. To locate f_m easily in spite of the presence of small irregularities in the data (which are partly due to small-scale variations of plasma and magnetic parameters during the frequency sweep), three conditions have to be met. First, the angle θ between the antenna and $\mathbf{B}$ must vary widely when the spacecraft spins; second, the gyrofrequency must be sufficiently large for the intraharmonic bands to be resolved accurately enough. Third, f_m should not be too close to the limits of the bands; otherwise, as may be seen in Figure 5, $\partial(k_\perp \rho_c)/\partial(\omega/\Omega)$ would be large, yielding large errors in the determination of ρ_c. For the first harmonic bands this requires L of the order of ρ_c.

These conditions are met in the examples shown in Figure 3, which are typical of the data acquired in the torus within about 10° of the magnetic equator. To illustrate the method, consider Figure 3*a*. One can see that the transition in the spin modulation behavior takes place at the frequency $f_m \approx 1.5 f_g$ in the first band, and $f_m \geq 2.5 f_g$ in the second band. The corresponding solution of the dispersion equation (Figure 5) is $k_\perp \rho_c \approx 1.3$; this value has been calculated with $f_p/f_g \approx 7.6$ but is virtually independent of this parameter. Substituting this value of $k_\perp$ in (13) with $L = 35$ m, we deduce the cold electron gyroradius

$$\rho_c \approx 1.3 \times L/3 \approx 15 \text{ m} \qquad (28)$$

This yields the cold electron temperature (using $f_g \approx 19$ kHz)

$$T_c \approx (2\pi f_g \rho_c)^2 m_e / k_B \approx 2 \times 10^5 \text{ K}$$

(at 1629 UT, $\lambda_m \approx -2.3°$, $R \approx 7.9\ R_J$).

The change in the spin modulation is easily determined with an uncertainty smaller than one period of $\sin^2\theta$, that is, one half spin period. During that time the receiver tuning frequency sweeps ≈2 kHz. In the above case this corresponds to an incertitude of 0.1 in ω/Ω, which translates to an uncertainty smaller than 40% in T_c. A much better precision might be achieved by determining the value of T_c for which the theoretical spin modulation fits best the whole data within the intraharmonic bands. It is important to note that the method, as implemented here, does not require any independent knowledge of the magnetic field direction: the absolute phase of the spin modulation with respect to the magnetic field is easily deduced from the observed modulation in the upper frequency part of the bands, where it varies as $\sin^2\theta$.

Applying this simple method to other spectra yields the variation of temperature in the torus along Ulysses trajectory, which was basically north-to-south, in contrast with the nearly equatorial Voyager 1 trajectory. Figure 8 shows the (15 min averaged) results so obtained from +11° to −11° magnetic latitude. The main trend is a temperature increase with distance from the magnetic (or centrifugal) equator. Typically, T_c increases from 1.3×10^5 K at $\lambda_m \approx 1.5°$ ($R \approx 7.7\ R_J$) to 2.9×10^5 K at latitude $\lambda_m \approx +11°$ ($R \approx 7.3\ R_J$) and, on the other side of the equator, to 2.5×10^5 K at $\lambda_m \approx -11°$ ($R \approx 8.5\ R_J$).

As remarked in Section 3.1, if the electron distribution is slightly anisotropic, these results refer to the temperature $T_{c\perp}$ perpendicular to the magnetic field.

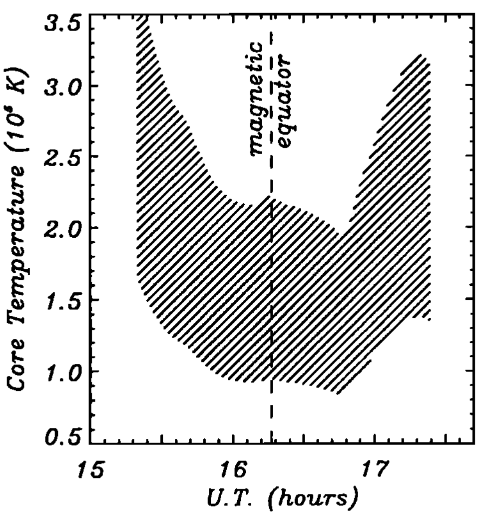

Fig. 8. Temperature (15 min averaged) as a function of time, deduced from the spin modulation of Bernstein waves from $\sim+11°$ to $-11°$ magnetic latitude along Ulysses trajectory in the torus (at $\sim 8\ R_J$ from Jupiter). The shaded region sketches the maximum error bars, whose present large values are due to the very simple method used here.

Ulysses crossed the magnetic equator near the outer boundary of the hot torus; in this region, the electron analyzers aboard Voyager (which were also sensitive to $T_\perp$, albeit for different reasons) gave temperatures of the same order, with a (somewhat irregular) temperature increase with Jovicentric distance [*Sittler and Strobel*, 1987]. Such a variation with R might explain a part of the increase found here towards negative latitudes, but not that found on the other side of the equator. Therefore, our results most probably indicate an actual temperature increase with latitude or distance from the magnetic (or centrifugal) equatorial plane.

It is difficult to study the spin modulation and to deduce the temperature at magnetic equator crossing, owing to the partial saturation of the receiver. But it is noteworthy that the noise level just below the plasma frequency appears at that time to be close to thermal noise without a magnetic field (exhibiting in particular a very small spin modulation and a nearly flat spectrum below the plasma frequency). From this level we have derived a temperature of $T_c \approx 10^5$ K, which is just slightly smaller than the value of 1.3×10^5 K obtained here at $\lambda_m \approx 1.5°$ (see Hoang et al., submitted manuscript, 1993) (where more complete results will be given).

4.2. *Midband Amplitudes: The Hot Population*

Let us now compare the spectral density in the middle of the bands (for $\theta \approx \pi/2$) with the theoretical estimate. We consider the region within $\sim 10°$ of the magnetic equator (excluding equator crossing), where the spin modulation allows a determination of the cold temperature. The midband amplitudes measured in this region for $\theta \approx \pi/2$ are $\sim 10^{-12}$ V^2 Hz^{-1} within a factor of 2, except when noise bursts are present. Using $k_\perp \rho_c \approx 1$ in the middle of the bands and the cold temperature deduced from the spin modulation, we find that the term $F_\perp(k_\perp L)/T_c^{1/2}$ in (23) is $\sim 4 \times 10^{-3}$ within a factor of 2. Substituting these parameters in (23), we obtain

$$T_h \approx 2 \times 10^7 \text{ K}$$

which is of the order of the hot electron temperature of ~ 1 keV found by [*Sittler and Strobel*, 1987] in the hot torus. This is a rather strong confirmation of the present interpretation and suggests that the order of magnitude of the hot temperature did not change in this region. However, we must keep in mind that we only made a rough estimate, which is strongly dependent on the hot population distribution. Using the comparison between theory and experiment to deduce precise parameters of the hot electrons would require further study.

We note in passing that in most of the region where we have estimated T_h, the spectrogram shows a bursty emission with a high-frequency cutoff just below $0.5 f_g$. This is best seen in the lower panel of Figure 1, near 10 kHz, between $\sim$1530 and $\sim$1700 UT (except close to the equator where the cutoff frequency is smaller), and in Figure 2*a*. The frequency of this emission is in the whistler range, but its scale of variation is too short to be resolved by the instrument, precluding unambiguous identification. Whistler waves were detected aboard Voyager at similar Jovicentric distances [*Coronoti et al.*, 1980], and found also aboard Ulysses at very low frequencies [*Farrell et al.*, this issue]. For electrons in cyclotron resonance ($kv_\parallel = \omega - \Omega$) with whistler waves, the energy of parallel motion is $E_\parallel = (\Omega/\omega)(1 - \omega/\Omega)^3 k_B T_c/\beta$, $k_B T_c/\beta$ being the magnetic energy per particle. The wave instability requires that these electrons have more perpendicular than parallel energy; for the special case of a bi-Maxwellian distribution the minimum temperature anisotropy is $T_{h\perp}/T_{h\parallel} = \Omega/(\Omega - \omega)$ [*Kennel and Petschek*, 1966].

At the maximum frequency $f \sim 0.5 f_g$ and with $\beta \sim 3 \times 10^{-3}$ (equation (3)), the parallel energy of ambient resonant electrons is (in temperature units) $E_\parallel/k_B \sim 80 T_c$, and the minimum anisotropy of a bi-Maxwellian producing whistler instability would be $T_{h\perp}/T_{h\parallel} \sim 2$, (which is not sufficient to make Bernstein waves unstable). With $T_c \sim 1.3 \times 10^5$ K this yields $E_\parallel/k_B \sim 10^7$ K, hence perpendicular energies of the same order as the hot temperature estimated above. These figures, however, must be taken with caution, since contrary to the case of Bernstein waves, the present whistler mode identification is not unambiguous, and the emission might come from a distant region.

4.3. *Spectral Minima: Deducing the Magnetic Field Strength*

Consider now the spectral minima at the gyroharmonics. Since the Doppler shift might be significant at the first ($n = 1$) harmonic, we only consider the $n > 1$ harmonics.

First, let us verify that the level corresponds to thermal noise. Consider the densest region explored by Ulysses, within $\pm 5°$ magnetic latitude, where we find values of the cold electron density and temperature which do not change very much. The measured level at the spectral minima is $\sim 10^{-14}$ V^2 Hz^{-1} within a factor of 2. In this region the plasma frequency is $f_p \approx 200$ kHz (Figure 1), and the temperature determined from the spin modulation remains near $T_c \approx 1 - 2 \times 10^5$ K. Substituting these parameters in

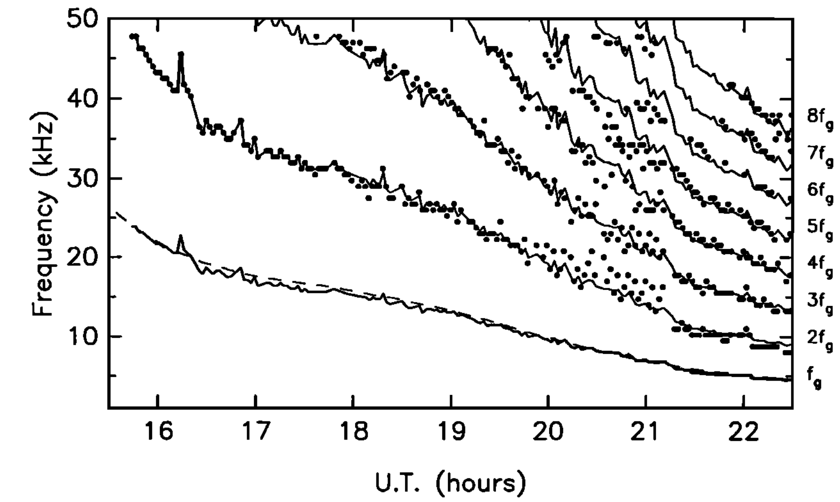

Fig. 9. Measured frequencies of the minima of the spectral shape (dots), together with the gyrofrequency and its harmonics computed by averaging the gyrofrequencies deduced from these minima (continuous lines). The gyrofrequency calculated from the magnetometer data (64-s averages; courtesy of A. Balogh) is shown for comparison as a dashed line.

(27), we find the theoretical order of magnitude of the thermal noise:

$$V_{\omega T}^2 \sim 0.5 - 1 \times 10^{-14} \text{ V}^2 \text{ Hz}^{-1}$$

in agreement with the measured level.

A very interesting point is that the gyrofrequency and thus the magnetic field strength can be derived from the frequencies of the spectral minima. Whereas individual determinations may be spoiled by possible noise bursts and by the spin modulation (and from 18 to ~2115 UT by additional shot noise due to a change in the antenna configuration), and cannot be more precise than the 0.75-kHz receiver bandwidth, a fairly good precision can be achieved by averaging over the gyrofrequencies deduced from the different harmonics. We have plotted in Figure 9 the gyroharmonics corresponding to the gyrofrequency deduced in this way, when at least two harmonics lie in the receiver range; dots show the measured frequencies of the spectral minima. For comparison, we have plotted the gyrofrequency calculated from the (64 s averaged) data of the magnetometer experiment on Ulysses [*Balogh et al.*, 1992]. Both determinations agree within a few percent.

5. Final Remarks

We have interpreted Ulysses electric field observations in the torus as quasi-thermal fluctuations in Bernstein waves. It may be noted that similar observations were carried out with the radio astronomy instrument aboard Voyager 1 and attributed to plasma instabilities [*Birmingham et al.*, 1981]. However, in that experiment the resolution of the gyroharmonic bands was insufficient, and the authors acknowledged the possibility that stable nonthermal features might have been observed.

An important result of the present study is that when the antenna is longer than roughly half the wavelength of Bernstein waves, the spectral density has a minimum when the antenna is normal to the magnetic field, contrary to what would be naively expected for longitudinal waves propagating perpendicular to **B**. This property is characteristic of filamental antennae and does not hold for dipoles made of two small spheres.

This counterintuitive behavior is due to the antenna response, which enhances the role of electrostatic waves whose wavelength along its direction is of the order of its length L; as a result, the direction of maximum sensitivity of long antennas is shifted at 90° from that of short dipoles (see N. Meyer-Vernet, manuscript in preparation, 1993). In analyzing electrostatic wave spectral densities one must never forget that the observed level is in general different from the actual plasma wave level and depends strongly on the antenna response function. This point, which is often forgotten in interpreting observations, may produce very different amplitudes, spectral shapes and apparent polarizations depending on the antenna length and geometry, even with the same basic phenomenon. Since in particular, the apparent electric field spectrum $E_\omega^2 = V_\omega^2/L^2$ decreases with the antenna length as $1/L^3$, the widespread tradition of describing the observations in terms of apparent electric field amplitudes (often without giving the associated antenna length) can be very misleading.

In practice, the antenna response plays an important role for Bernstein waves when the antenna length is larger than the cold electron gyroradius ρ_c. *Sentman* [1982] first noted the importance of this point when interpreting the absolute intensity and spectral shape. A similar situation holds around the plasma frequency in the absence of a magnetic field when the antenna length is larger than the Debye length [*Meyer-Vernet and Perche*, 1989]; it has a similar physical origin, although the response function is in that case different since the field is isotropic instead of gyrotropic.

We have found that the normalized frequency f/f_g at which the spin modulation reverses is a rather simple function of L/ρ_c (through Bernstein's dispersion equation). This provides a new method to measure the cold electron temperature aboard a spinning spacecraft when the spin axis makes a significant angle with the local magnetic field. This measurement is nearly independent of the hot electrons when they only make up a very small percentage of the total density. Contrary to usual thermal noise spectroscopy

[*Meyer-Vernet and Perche*, 1989], it is also independent of any gain calibration, and even of the plasma frequency if it is large enough. It does not require an independent measurement of the magnetic field, except if the latter varies very rapidly.

Our results might also serve to study the plasma instabilities for which $|k_{\parallel}| \ll k_{\perp}$, since the response function (7) permits to deduce the wavelength from the observed spin modulation.

In the ideal case when the electron distribution is a sum of two Maxwellians with $n_h/n_c \ll 1$ and $T_h/T_c \gg 1$ the absolute spectral density might be used to deduce T_h (T_c being measured from the spin modulation). In this paper we have not tried to deduce a precise value of T_h because this determination is very sensitive to the hot electron distribution, and precise results require complex numerical computations. We only note that the amplitudes measured in the torus agree in order of magnitude with the quasi-thermal noise calculated in a plasma whose electron distribution is made of two Maxwellians with a hot temperature in the kiloelectron volt range.

Our main result, obtained at $\sim 8\ R_J$ from Jupiter, is that the cold electron temperature ($T_{c\perp}$) increases (nonmonotonocally) with latitude, by a factor of ~ 2 over $\sim\pm 10°$ latitude (i.e., a distance of $\sim 1.3\ R_J$ from the magnetic equatorial plane). It may be noted that the particle analyzers aboard Voyager 1 [*Sittler and Strobel*, 1987] gave some hints to a slight temperature increase with latitude, although the spacecraft trajectory was not adequate to study such an effect.

The latitudinal temperature increase found here is far too large to be explained by the variation in perpendicular energy expected along a line of force due to magnetic moment conservation, since the magnetic field change over 10° latitude is very small. The electrons are mainly driven by the ambipolar electric field which tends to confine them at low (centrifugal) latitudes, making them follow the ions in the presence of the corotational centrifugal force. Their Coulomb free path being much larger than the scale height, the situation has some similarities with a collisionless atmosphere confined by gravity. In that case, if the velocity distribution is Maxwellian, the temperature does not change with altitude. If, however, the distribution is not Maxwellian (being for example a Kappa function differing only slightly from a Maxwellian at low energies, but decreasing less steeply at high energies), the tendency of colder electrons to be more confined by the potential than the hot ones makes the effective temperature increase with height as the density decreases [*Scudder*, 1992]. (Also, the density at large distances decreases more gently than a Gaussian.) We have not yet explored the possibility of a similar effect being at work here.

A by-product of Bernstein wave measurements below f_{UH} is the magnetic field strength, since the spectral shape has well-defined minima at the gyroharmonics. This shows that a passive radio experiment can serve both as an in situ thermometer and magnetometer when it is not measuring radio emissions. If $f_g \ll f_p$ (with $n_h \ll n_c$ and $L > L_D$) as holds in Io's torus, the peak at $f_p \approx f_{UH}$ also gives the plasma density. This condition does not hold farther from Jupiter; one should then see additional spectrum maxima at the first f_Q frequencies (for which $k_{\perp}L$ is not too large), sufficiently distinct from f_{UH}. This may be used to deduce the plasma frequency, using Bernstein's dispersion equation, for instance to measure the density in regions of Jupiter's environment where there were no particle measurements on Ulysses and when different interpretations of the relaxation sounder data [*Stone et al.*, 1992*b*] gave conflicting results.

Acknowledgments. The URAP experiment is a joint project of NASA GFSC, Observatoire de Paris, CRPE, and University of Minnesota. The Principal Investigator is R. G. Stone. The French contribution was financed by the Centre National d'Etudes Spatiales and partly by the CNRS. We are very grateful to the team of engineers and technicians who designed and built the radio receiver, whose great sensitivity and stability made possible the study of plasma thermal noise in various environments. Our sincere thanks are also due to our colleagues at GSFC for sharing their data reduction system with us and to A. Balogh, Principal Investigator and R. J. Forsyth, Co-Investigator, on the magnetometer experiment for kind permission to use their data. We are grateful to J.-L. Steinberg for numerous comments and helpful suggestions on the manuscript.

The Editor thanks R. MacDowall and D. A. Gurnett for their assistance in evaluating this paper.

REFERENCES

Abramowitz, M., and I. A. Stegun, *Handbook of Mathematical Functions*, p. 480, Dover, New York, 1970.

Balogh, A., et al., Magnetic field observations during the Ulysses fly-by of Jupiter, *Science*, *257*, 1515, 1992.

Balmain, K. G., The impedance of a short dipole antenna in a magnetoplasma, *IEEE Trans. Antennas Propag.*, *AP-12*, 605, 1964.

Belmont, G., Characteristic frequencies of a non-Maxwellian plasma: A method for localizing the exact frequencies of magnetospheric intense natural waves near f_{pe}, *Planet. Space Sci.*, *29*, 1251, 1981.

Bernstein, I. B., Waves in a plasma in a magnetic field, *Phys. Rev.*, *109*, 10, 1958.

Birmingham, T. J., J. K. Alexander, M. D. Desch, R. F. Hubbard, and B. M. Pedersen, Observations of electron gyroharmonic waves and the structure of Io torus, *J. Geophys. Res.*, *86*, 8497, 1981.

Chateau, Y. F., and N. Meyer-Vernet, Electrostatic noise in non-Maxwellian plasmas: Generic properties and kappa distributions, *J. Geophys. Res.*, *96*, 5825, 1981.

Christiansen, P. J., et al., Geos-1 observations of electrostatic waves, and their relationship with plasma parameters, *Space Sci. Rev.*, *22*, 383, 1978.

Coronoti, F. V., F. L. Scarf, C. F. Kennel, W. S. Kurth, and D. A. Gurnett, Detection of Jovian whistler mode chorus: Implication for the Io torus aurora, *Geophys. Res. Lett.*, *7*, 45, 1980.

Farrell, W. M., R. J. MacDowall, R. A. Hess, M. L. Kaiser, M. D. Desch, and R. G. Stone, An interpretation of the broadband VLF waves near the Io torus as observed by Ulysses, *J. Geophys. Res.*, this issue.

Gradshteyn, I. S., and I. M. Ryshik, *Table of Integrals, Series and Products*, Academic, San Diego, Calif., 1980.

Kennel, C. F., and H. E. Petschek, Limit on stably trapped particle fluxes, *J. Geophys. Res.*, *71*, 1, 1966.

Kennel, C. F., F. L. Scarf, R. W. Fredricks, J. H. McGehee, and F. V. Coronoti, VLF electric field observations in the magnetosphere, *J. Geophys. Res.*, *75*, 6136, 1970.

Kennel, C. F., and M. Ashour-Abdalla, Electrostatic waves and the strong diffusion of magnetospheric electrons, in *Magnetospheric plasma physics*, edited by A. Nishida, p. 245, Center for Academic Publications, Tokyo, 1982.

Kurth, W. S., D. D. Barbosa, D. A. Gurnett, and F. L. Scarf, Electrostatic waves in the Jovian magnetosphere, *Geophys. Res. Lett.*, *7*, 57, 1980.

Kurth, W. S., F. L. Scarf, D. A. Gurnett, and D. D. Barbosa, A survey of electrostatic waves in Saturn's magnetosphere, *J. Geophys. Res.*, *88*, 8959, 1983.

Kurth, W. S., D. D. Barbosa, D. A. Gurnett, and F. L. Scarf,

Electrostatic waves in the magnetosphere of Uranus, *J. Geophys. Res.*, *92*, 15,225, 1987.
Meyer, P., and N. Vernet, Impedance of a short antenna in a warm magnetoplasma, *Radio Sci.*, *9*, 409, 1974.
Meyer, P., N. Vernet, and P. Lassudrie-Duchesne, Theoretical and experimental study of the effect of the sheath on an antenna immersed in a warm isotropic plasma, *J. Appl. Phys.*, *45*, 700, 1974.
Meyer-Vernet, N., On natural noises detected by antennas in plasmas, *J. Geophys. Res.*, *84*, 5373, 1979.
Meyer-Vernet, N., and C. Perche, Tool kit for antennae and thermal noise near the plasma frequency, *J. Geophys. Res.*, *94*, 2405, 1989.
Nakatani, D. T., and H. H. Kuehl, Input impedance of a short dipole antenna in a warm anisotropic plasma, 1, Kinetic theory, *Radio Sci.*, *11*, 433, 1976.
Scudder, J. D., On the causes of temperature change in inhomogeneous low-density astrophysical plasmas, *Astrophys. J.*, *398*, 299, 1992.
Scudder, J. D., and E. C. Sittler, A survey of the plasma electron environment of Jupiter: A view from Voyager, *J. Geophys. Res.*, *86*, 8157, 1981.
Sentman, D. D., Thermal fluctuations and the diffuse electrostatic emissions, *J. Geophys. Res.*, *87*, 1455, 1982.
Shaw, R. R., and D. A. Gurnett, Electrostatic noise bands associated with the gyrofrequency and plasma frequency in the outer magnetosphere, *J. Geophys. Res.*, *80*, 4259, 1975.
Sittler, E. C., Jr., and D. F. Strobel, Io plasma torus electrons: Voyager 1, *J. Geophys. Res.*, *92*, 5741, 1987.
Stone, R. G., et al., The unified radio and plasma wave investigation, *Astron. Astrophys. Suppl. Ser.*, *92*, 291, 1992*a*.
Stone, R. G., et al., Ulysses radio and plasma wave observations in the Jupiter environment, *Science*, *257*, 1524, 1992*b*.

S. Hoang, N. Meyer-Vernet, and M. Moncuquet, Département de Recherche Spatiale, CNRS URA 264, Observatoire de Paris, 92195 Meudon Cedex, France.

(Received March 16, 1993;
revised July 12, 1993;
accepted July 12, 1993.)